Since January 2020 Elsevier has created a COVID-19 resource centre with free information in English and Mandarin on the novel coronavirus COVID-19. The COVID-19 resource centre is hosted on Elsevier Connect, the company's public news and information website.

doi:10.1016/j.jmb.2007.05.058 J. Mol. Biol. (2008) 375, 511–528

JMB

Available online at www.sciencedirect.com

ScienceDirect

ELSEVIER

Characterization of the Mechanical Unfolding of RNA Pseudoknots

Lisa Green[1], Chul-Hyun Kim[2], Carlos Bustamante[3,4] and Ignacio Tinoco Jr[1]*

[1]*Department of Chemistry University of California Berkeley, Berkeley CA 94720, USA*

[2]*Department of Chemistry and Biochemistry, California State University, East Bay Hayward, CA 94542, USA*

[3]*Department of Physics and Molecular and Cell Biology University of California Berkeley, Berkeley CA 94720, USA*

[4]*Howard Hughes Medical Institute, University of California, Berkeley Berkeley, CA 94720, USA*

**Corresponding author*

The pseudoknot is an important RNA structural element that provides an excellent model system for studying the contributions of tertiary interactions to RNA stability and to folding kinetics. RNA pseudoknots are also of interest because of their key role in the control of ribosomal frameshifting by viral RNAs. Their mechanical properties are directly relevant to their unfolding by ribosomes during translation. We have used optical tweezers to study the kinetics and thermodynamics of mechanical unfolding and refolding of single RNA molecules. Here we describe the unfolding of the frameshifting pseudoknot from infectious bronchitis virus (IBV), three constituent hairpins, and three mutants of the IBV pseudoknot. All four pseudoknots cause −1 programmed ribosomal frameshifting. We have measured the free energies and rates of mechanical unfolding and refolding of the four frameshifting pseudoknots. Our results show that the IBV pseudoknot requires a higher force than its corresponding hairpins to unfold. Furthermore, its rate of unfolding changes little with increasing force, in contrast with the rate of hairpin unfolding. The presence of Mg^{2+} significantly increases the kinetic barriers to unfolding the IBV pseudoknot, but has only a minor effect on the hairpin unfolding. The greater mechanical stability of pseudoknots compared to hairpins, and their kinetic insensitivity to force supports the hypothesis that −1 frameshifting depends on the difficulty of unfolding the mRNA.

Keywords: RNA pseudoknots; single molecules; frameshifting; laser tweezers; force unfolding

Introduction

The pseudoknot is a simple tertiary structure motif found in a wide range of RNA molecules; because of their structure, pseudoknots can give insight into how tertiary and secondary RNA structures contribute to the stability and kinetics of folding. Among the many different types of pseudoknots classified by their topology, the most common is the H-type pseudoknot.[1] The H-type pseudoknot consists of a hairpin stem (stem 1) with a second stem formed by the downstream region that base-pairs with the loop of stem 1. H-type pseudoknots are found in many kinds of RNA molecules including messenger RNA,[2] ribosomal RNA,[3] transfer-messenger RNA,[4] catalytic self-splicing RNA[5,6] and viral genomic RNA.[7] While RNA pseudoknots often serve as structural elements helping to stabilize complex three-dimensional structures, they also perform an active role as essential elements in the regulation of several biological processes. Deletion of key pseudoknots can disrupt activity in telomerase[8,9] and catalytic ribozymes.[10–13] Pseudoknots also play a role in initiation of internal ribosome entry translation,[14,15] binding of ribosomal proteins to RNA,[16–18] and controlling the translational frame during protein synthesis.[19–24]

We focus on frameshifting mRNA pseudoknots that are involved in translational control of viral proteins *via* −1 programmed ribosomal frameshifting (−1 PRF). Here, we characterize the mechanical unfolding and refolding of the pseudoknot that

Abbreviations used: IBV, infectious bronchitis virus; −1 PRF, −1 programmed ribosomal frameshifting; WLC, worm-like-chain.

stimulates −1 PRF in the infectious bronchitis virus (IBV), three mutant pseudoknots that also stimulate −1 PRF, and three related hairpin molecules with the same stems but lacking the tertiary base-pairing of their related pseudoknots. Our goal is to evaluate the nature of tertiary interactions in RNA and to gain insight into the mechanism of frameshifting by these pseudoknots.

Currently, it is possible to predict secondary structure from a nucleic acid sequence based on experimentally derived thermodynamic values.[25,26] However, the goal of predicting tertiary structure from an RNA sequence has yet to be achieved. To meet this goal, a better understanding of the contributions of tertiary interactions to RNA stability and folding kinetics is crucial. Comparison of the folding and unfolding characteristics of an RNA pseudoknot and its corresponding hairpins provides a simple system for quantifying the contributions of tertiary interactions. As many *in vivo* RNA unfolding events are accomplished by molecular motors that exert force on the RNA,[27] the effects of tertiary structure on the mechanical characteristics of RNA unfolding may have a direct relevance to the biological functions of RNA. Extensive studies on the folding characteristics of pseudoknots and other RNA structures using thermal or chemical denaturation methods have provided much useful information.[23,28–34] However, mechanical unfolding differs significantly from these methods. Thermal and chemical denaturation act upon an RNA globally, thus, unfolding can begin with any of the base-pairs. In contrast, mechanical force acts locally upon the 3′ and 5′ ends of an RNA hairpin; the base-pairs of a hairpin unfold sequentially along the stem towards the loop. Furthermore, force applied to the 3′ and 5′ ends of an RNA will be experienced differently by a secondary structure such as a hairpin, than it will be experienced by a tertiary structure such as a pseudoknot. As illustrated by the arrows indicating direction of force in Figure 1, a hairpin will experience a localized tensile force whereas a pseudoknot will experience a shearing force across its structure. Mechanical unfolding of RNA, whether carried out *in vivo* by molecular machines or carried out *in vitro* by optical tweezers, is influenced by tertiary interactions in a manner that is not revealed by thermal and chemical unfolding. Thus, mechanical unfolding and refolding of the tertiary conformations of RNA can provide insight relevant to *in vivo* biological processes.

Investigations into the properties of frameshifting pseudoknots can improve our understanding of their specific role in the frameshifting process. Minus-1 programmed ribosomal frameshifting is a recoding mechanism that regulates the relative expression of proteins encoded by polycistronic mRNA in overlapping reading frames in viral mRNA. This process regulates protein levels in various viruses including IBV, human immunodeficiency virus (HIV) and severe acute respiratory syndrome (SARS),[19–24]) and is crucial for viral replication. Variation in the viral protein ratio substantially reduces the infectivity of viruses,[35] which makes the −1 PRF process an attractive target for antiviral therapy.

Despite extensive structural and functional characterization,[20,21,23,24,36] the mechanism by which pseudoknots regulate −1 PRF remains unknown. Previous studies have identified three RNA components that determine the efficiency of −1 PRF: a slippery sequence, a linker region and a downstream structural element. The downstream structure is most often a pseudoknot.[21] The frameshifting efficiency shows a wide range of variability among pseudoknots; alterations in the structure of the pseudoknot can substantially affect this frameshifting efficiency. Previous studies have established that the thermodynamic stability is not correlated with frameshifting efficiency.[37,38] Though a recent paper reporting on the mechanical unfolding of two mutant pseudoknots presents data that suggest the magnitude of the average unfolding force may be correlated with frameshifting efficiency,[39] it is clear that the regulation of ribosomal frameshifting is not simply a matter of thermodynamics. It has been proposed that the kinetics of unfolding may dictate frameshifting efficiency,[23] and in particular, the kinetics of unfolding along a mechanical reaction coordinate, but these properties have not been characterized for frameshifting pseudoknots until now.

As the −1 PRF signal is a part of the mRNA that is unfolded by the ribosome during translation, the pseudoknot is exposed to mechanical force during the frameshifting event. Therefore, the structural characteristics of a pseudoknot that determine frameshifting efficiency may be related to its mechanical properties. The possibility that −1 PRF is dependent on the mechanical tension induced by a folded pseudoknot was a fundamental component of the torsional restraint model[36] and this hypothesis was recently further strengthened by cryo-electron microscopic imaging of eukaryotic ribosomes complexed with mRNA containing a frameshifting pseudoknot.[40] Accordingly, using mechanical force to unfold and refold individual pseudoknots can provide useful insight into the role that the mechanical properties of pseudoknots play in the frameshifting process. Of course, we recognize that chemical interactions between the pseudoknot and the translational apparatus will also play a role.

Mechanical unfolding and refolding of a single molecule of RNA can be accomplished using optical tweezers; thermodynamic and kinetic information can thus be obtained.[42–45] Here, we use optical tweezers to mechanically unfold and refold a minimal wild-type construct of the IBV pseudoknot and three constituent hairpins, in order to compare the unfolding and refolding characteristics of secondary and tertiary structure on a single-molecule level. We also characterized the unfolding and refolding behavior of three frameshifting mutants of the IBV pseudoknot that span a range of frameshifting efficiencies. The differences in mechanical properties

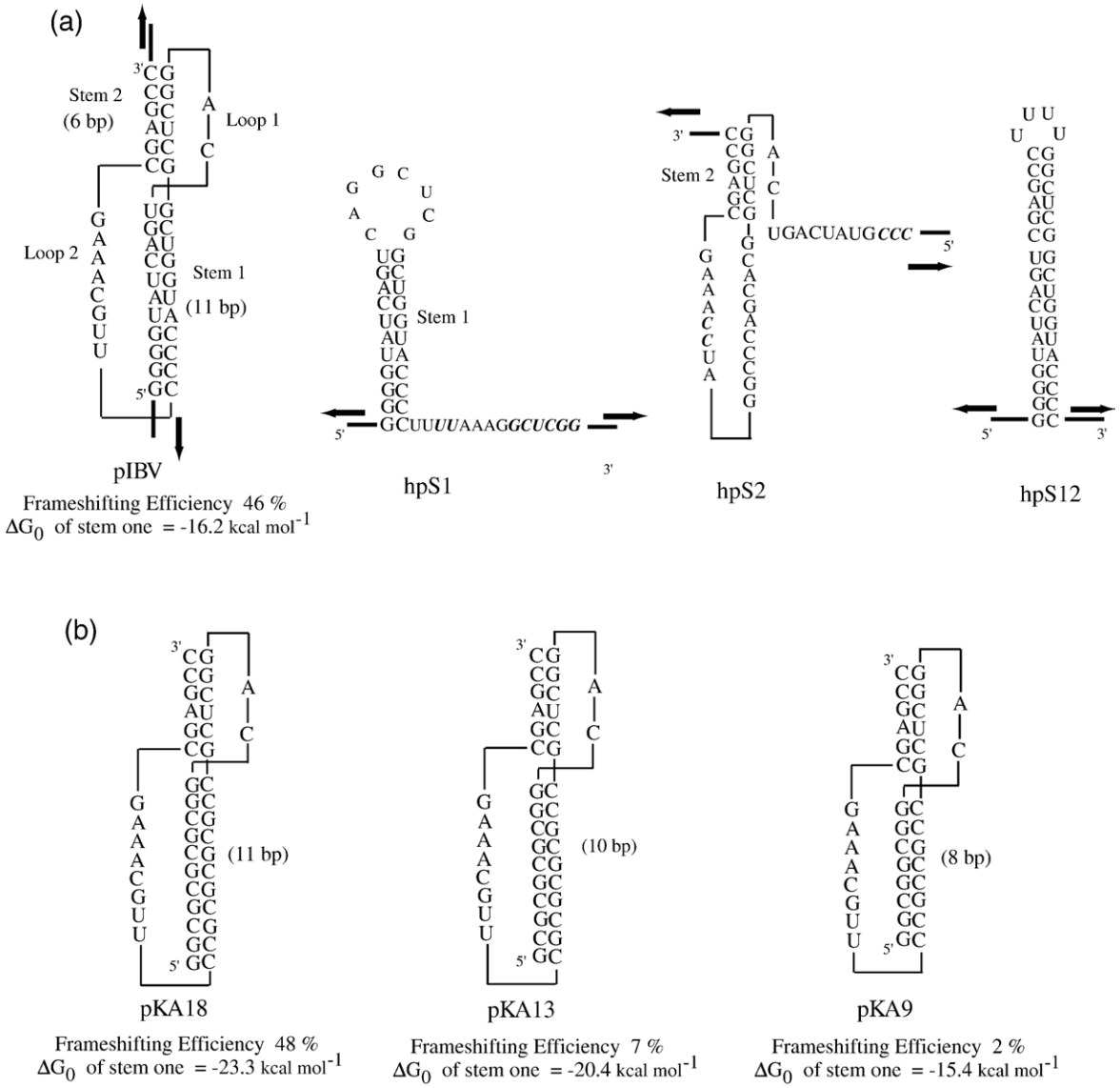

Figure 1. RNA constructs used for single-molecule optical tweezers experiments. (a) IBV pseudoknot (pIBV) and its related hairpin constructs. The nucleotides shown in bold italic font were mutated from the pIBV sequence to prevent the formation of other secondary structures. The ΔG_0 value of stem 1 as calculated using the nearest-neighbor hypothesis is shown for all molecules. The measured frameshifting efficiency[37] is shown for pIBV. The arrows indicate the direction of applied force. (b) The constructs of mutant IBV pseudoknots. The stem 1 sequence of pIBV was completely replaced by G•C base-pairs. The ΔG_0 value of stem 1 as calculated using the nearest-neighbor hypothesis and the measured frameshifting efficiency[37] is shown for the mutant pseudoknots.

of the wild-type and mutant pseudoknots, and between the pseudoknots and hairpins can shed light on the role of these properties in the frameshifting efficiency of pseudoknots. These studies also further our understanding of the contributions of tertiary interactions to RNA folding.

A recent mechanical unfolding experiment on two pseudoknots, entitled "Correlation between mechanical strength of messenger RNA pseudoknots and ribosomal frameshifting",[39] found that the pseudoknot with the higher frameshifting efficiency (14% *versus* 6%) unfolded at a higher force. Our studies on the thermodynamics, kinetics, and mechanical properties of a wild-type plus three mutant pseudoknots show no general correlation exists between frameshifting efficiency and mechanical strength (unfolding force).

Results

Experimental design

The sequences and structures of the seven RNA molecules used in this study: IBV pseudoknot (pIBV), three of its mutant pseudoknots and three related hairpins, are shown in Figure 1. Infectious bronchitis virus was one of the first virus shown to utilize ribosomal frameshifting.[46] We chose the IBV

pseudoknot as our model system because it has been well-characterized and there is a wealth of data from the numerous studies which have used it as a model for understanding ribosomal frameshifting.[37,46–50]

We designed the hairpins from the constituent parts of pIBV (Figure 1(a)). Hairpins hpS1 and hpS2 model partially folded conformations of pIBV; they contain the base-pairs of stem 1 and stem 2, respectively, with changes in the pIBV sequence to ensure that the other stem does not form. Comparison between pIBV and the hairpins was used to determine whether the pIBV construct formed a partially folded conformation instead of folding into the native pseudoknot. The hairpin hpS12 consists of the base-pairs that are present in stem 1 plus stem 2 of pIBV.

The wild-type IBV pseudoknot has been shown to have a frameshifting efficiency of 46% in a rabbit reticulocyte frameshifting assay.[37] The three mutant pseudoknots used here, pKA18, pKA13 and pKA9, were originally designed and described by the Brierley laboratory and their respective frameshifting efficiencies were determined to be 48%, 7% and 2%.[37] All four pseudoknots are identical except for variation in stem 1 (see Figure 1(b)). Stem 1 of the mutants consists of G•C base-pairs only; the lengths of stem 1 vary: 11 bp for pIBV and pKA18, 10 bp for pKA13, and 8 bp for pKA9.

RNA molecules were prepared as constructs for single molecule pulling experiments by attaching RNA/DNA hybrid spacers approximately 500 bp long (referred to as handles) between the RNA structures and two micro-beads as described[41] (see Methods and Materials and Figure 2). One bead is held in an optical trap and the other is held on the tip of a micropipette by suction. Force is exerted on the molecule by moving the micropipette away from the optical trap.

Here, we have used two types of mechanical unfolding and refolding experiments, force-ramp and constant force.[51] Force-ramp experiments allow one to observe unfolding/refolding by stretching/relaxing an RNA molecule with a force increasing/decreasing at a constant rate. Constant force experiments involve holding the molecule at a given force and monitoring unfolding and refolding events. In both types of experiments, the size of the transitions is measured as a change in the end-to-end molecular extension.

Force-ramp experiments were done at rates of 2 pN s^{-1} – 20 pN s^{-1} in a magnesium buffer (20 mM Tris, 50 mM NaCl, 5 mM $MgCl_2$ (pH 7.5)) and in an EDTA buffer (20 mM Tris, 50 mM NaCl, 5 mM EDTA (pH 7.5)). Constant force experiments were performed in a magnesium buffer containing KCl instead of NaCl (20 mM Tris, 50 mM KCl, 5 mM $MgCl_2$ (pH 7.5)). The difference in the identity of the monovalent cation was found to have a negligible effect on the RNA folding reactions. Force-ramp experiments performed on pIBV and hpS12 in the KCl magnesium buffer yielded data that were not statistically different from the data collected in the NaCl magnesium buffer.

The IBV pseudoknot in comparison with three constituent hairpins

The unfolding and refolding processes of pIBV and the three hairpins were characterized for two purposes: in order to confirm that the pIBV construct does in fact fold correctly and also to investigate the differences in the folding characteristics due to the contributions of tertiary structure.

Pulling one RNA molecule by force: the force-extension curve of an RNA molecule

In force-ramp experiments, the molecule is stretched and relaxed by moving the pipette at a constant rate; examples of these force-extension curves are shown in Figures 3 and 4. In the low force regime the shape of the curve is the result of stretching the RNA–DNA hybrid handles; the curve aligns well with pulling curves generated using the worm-like-chain (WLC) model.[52] The sharp increase in extension and decrease in force observed in the

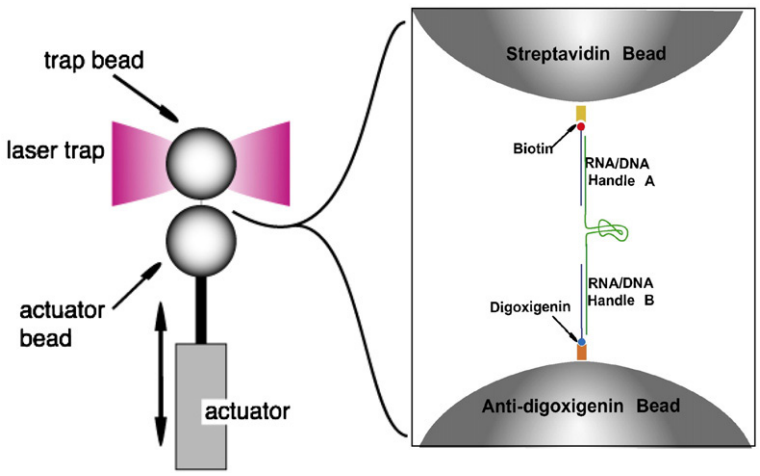

Figure 2. Diagram of a single-molecule optical tweezers experiment. An RNA construct is held between two beads. One bead is trapped in a focused laser trap and the other bead is held on the tip of a movable pipette (actuator). Through the movement of an actuator, the RNA construct can be stretched or relaxed between the beads. An RNA construct consists of RNA flanked with RNA–DNA hybrid handle regions (Inset). The handles are designed such that the 3′ end of the one handle is biotinylated (handle A) and the 5′ end of the other handle is functionalized with digoxigenin. Through biotin-streptavidin and digoxigenin and anti-digoxigenin antibody interactions, the RNA construct can be held between a streptavidin-coated bead and an anti-digoxigenin antibody-coated bead.

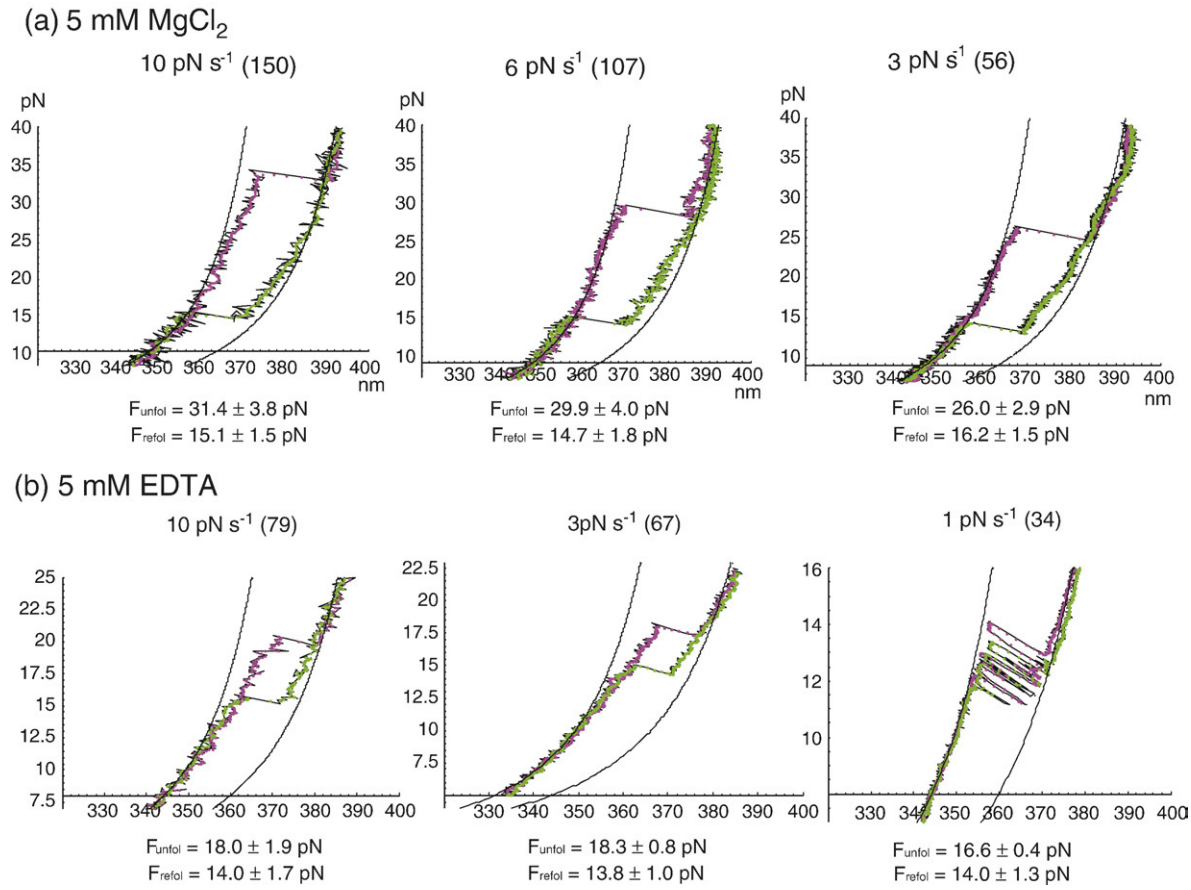

Figure 3. Force-extension curves of the IBV pseudoknot (pIBV). One representative force-extension curve at three different pulling rates is shown (a) in the presence of Mg^{2+} and (b) in the absence of Mg^{2+}. The unfolding curves are in magenta, the refolding curves are in dark green. For each curve, the x axis is the molecular end-to-end distance between two beads (nm) and the y axis is the pulling force that is exerted on each RNA construct (pN). Each force extension curve was aligned with a theoretically calculated (worm-like-chain) force-extension curve (two black lines) of the DNA–RNA handles with the corresponding number of its single-stranded nucleotides. The left side curve is for the DNA–RNA handles with a folded RNA and the right side curve is for the DNA–RNA handles with an unfolded RNA. Average unfolding forces and refolding forces with standard deviations are listed. The numbers in parentheses are the number of force-extension curves used to calculate each average unfolding and refolding force.

unfolding curve is referred to as an "unfolding rip" and is the result of unfolding the RNA structure in between the handles. Similarly, the sharp decrease in extension and increase in force observed in the refolding curve is referred to as a "refolding zip" and is the result of the RNA molecule folding into its secondary/tertiary conformation from its single-stranded unfolded state. The slope of a rip or zip is approximately equal to the spring constant of the optical trap. Hysteresis between the trajectories of the folding and unfolding curves indicates that processes are irreversible at these pulling rates.

The force-extension curves of pIBV: the role of Mg^{2+} in the tertiary interactions of the pseudoknot

As shown in Figure 1, pIBV consists of an 11 bp stem 1 and a 6 bp stem 2 with a two-nucleotide loop 1 and an eight-nucleotide loop 2. The force-extension curves of pIBV at various pulling rates are shown in Figure 3. To characterize the role of Mg^{2+} in the unfolding and refolding of pIBV, force-ramp experiments were done in the presence and absence of Mg^{2+}. As shown in Figure 3(a), in 5 mM $MgCl_2$, pIBV shows a single unfolding transition with an average length of 16(±1.5) nm (Table 1). This indicates that in the presence of Mg^{2+}, pIBV unfolds through rupturing of one compact conformation rather than the sequential unfolding of two constituent stems. The curves are reasonably well aligned with two calculated curves of the WLC model based on the folded and unfolded pseudoknot conformations. The average unfolding force and the distribution of unfolding forces both show a strong dependence on the pulling rate. The molecule unfolds at a high force range at fast pulling rates (around 31 pN at 10 pN s^{-1}) with a wide distribution of unfolding forces (SD, 3.8 pN), whereas it unfolds around 26 pN at 3 pN s^{-1} with a narrower distribution (SD, 2.9 pN). As shown in Figure 3(a), the pIBV pulling curves show a large hysteresis between

unfolding and refolding transitions even at the slowest pulling rate. This phenomenon indicates that the unfolding and refolding process of this molecule is slow compared with the pulling rates.

The force-extension curves of pIBV in the absence of Mg^{2+} (5 mM EDTA), also show a single unfolding rip, but the average unfolding force is much lower with a smaller length of the rips compared with

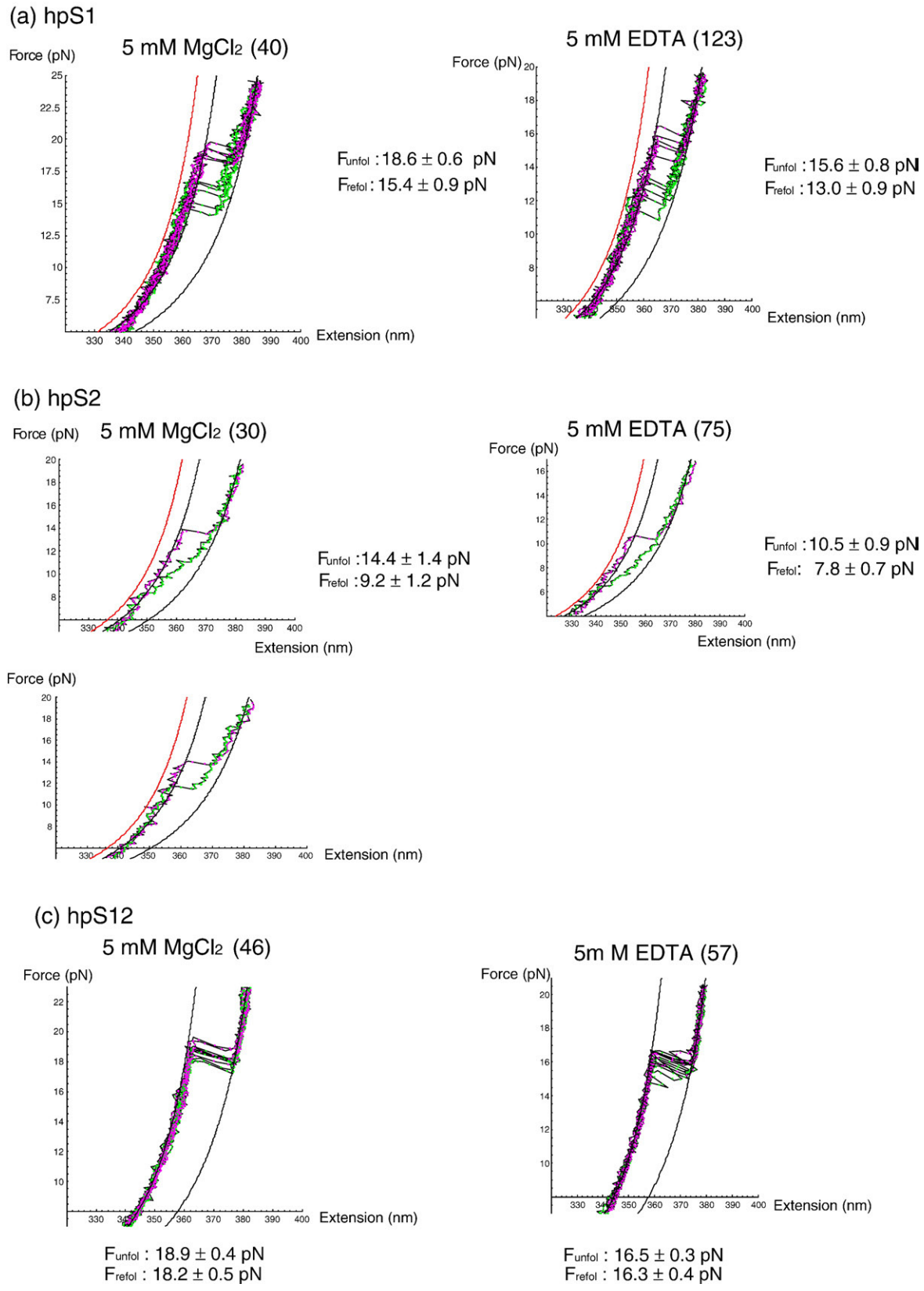

Figure 4 (*legend on next page*)

Table 1. The characteristics of the force-extension curves of the IBV pseudoknot (pIBV) and its related hairpins

	5 mM $MgCl_2$						5 mM EDTA					
	10 pN s^{-1}		3 pN s^{-1}				10 pN s^{-1}		3 pN s^{-1}			
	F_{unfol}	F_{refol}	F_{unfol}	F_{refol}	ΔX_u	ΔX_r	F_{unfol}	F_{refol}	F_{unfol}	F_{refol}	ΔX_u	ΔX_r
pIBV (68–79[a])	31.4±3.8	15.1±1.5	26.0±2.9	16.2±1.5	16±1.5	13±1.8	18.0±1.9	14.0±1.7	18.3±0.8	13.8±1.0	9±1.0	10±1.1
hpS12 (25–88[a])	21.4±0.9	19.6±1.5	18.8±0.4	18.6±0.4	15±1.1	15±1.1	18.5±0.4	18.0±0.5	16.7±0.3	16.5±0.3	15±0.8	15±1.1
hpS1 (52–124[a])	19.0±0.9	14.9±1.1	18.2±0.8	15.1±1.1	11±1.1	10±1.1	15.9±0.8	12.9±1.1	15.2±0.5	13.6±0.6	10±1.1	9±0.9
hpS2 (28–84[a])	15.7±1.4	N/A[b]	14.6±1.5	7.9±1.2[c]	10±2.0	6±0.9	11.4±1.2	8.3±0.4[d]	9.6±0.9	7.2±0.8[e]	10±1.4	7±0.8

F_{unfol}, average unfolding force (pN). F_{refol}, average refolding force (pN).
ΔX_u, Average values of the width of unfolding rips (nm). ΔX_r, Average values of the width of refolding zips (nm).
[a] Range of the number of pulling curves used to calculate the listed average values.
[b] No clear refolding zips were detected.
[c] Only 30 curves show clear refolding zips.
[d] Only three curves show clear refolding zips.
[e] Only 46 curves show clear refolding zips.

those observed in the presence of Mg^{2+}. At the slowest unfolding rate (1 pN s^{-1}), the molecule hops between folded and unfolded conformations. As shown in Figure 3(b), the unfolding curves deviate significantly from the WLC calculated curve before the rip, which indicates a part of pIBV (presumably stem 2) is unfolded before the rip occurs. We attribute the observed rip (9±1.0 nm; Table 1) in each curve to the unfolding of stem 1. In the absence of Mg^{2+}, the tertiary interactions that maintain the pseudoknot conformation are apparently very weak, and thus the shorter stem 2 may not be stable enough to show a discrete unfolding rip.

In contrast to the unfolding in the presence of Mg^{2+}, the unfolding of pIBV in its absence occurs at a significantly lower force and the distribution of unfolding forces is narrower (Table 1). Furthermore, in the absence of Mg^{2+} the average unfolding force does not show strong dependence on the pulling rate (about 18 pN for both 10 pN s^{-1} and 3 pN s^{-1}). Though the unfolding/refolding processes are irreversible with and without Mg^{2+}, the degree of hysteresis is noticeably decreased in the absence of Mg^{2+} (average unfolding force 18 pN and average refolding force 14 pN at 3 pN s^{-1}).

The force-extension curves of hpS1 and hpS2: does pIBV form a pseudoknot?

A previous study of the IBV pseudoknot confirmed that it folds into the structure shown in Figure 1 by using chemical and enzymatic probing.[37] In order to check that the pIBV construct actually forms a pseudoknot in our tweezers experiments, we compared the unfolding and refolding characteristics of pIBV to those of hpS1 and hpS2. If the pIBV construct forms a partially folded conformation instead of the pseudoknot, it would likely form a hairpin containing either stem 1 or stem 2 (hpS1 or hpS2). Therefore, comparison between the force-extension curves of pIBV and those of hpS1 and hpS2 indicates whether pIBV fails to fold into the expected pseudoknot conformation.

Force-ramp experiments were done on the hairpins hpS1 and hpS2 in the same conditions used for pIBV. The hairpin hpS1 mimics stem 1 of pIBV (Figure 1(a)). The force-extension curves for hpS1 in the presence of Mg^{2+} (Figure 4(a)) show a single unfolding rip. The average width of the unfolding rips is 11(±1.1) nm (Table 1), which is consistent with the number of nucleotides released on unfolding its stem. As shown in Figure 4(a), the unfolding forces of hpS1 have a narrow distribution around 19 pN in the presence of Mg^{2+} and around 16 pN in the absence of Mg^{2+} at the pulling rate of 5 pN s^{-1}. Unlike pIBV data taken in Mg^{2+} buffer, hpS1 data in the same conditions does not show a strong dependence of average unfolding force on pulling rate. Although hpS1 shows an increase in both the average unfolding force and in the size of the hysteresis in the presence of Mg^{2+}, the change is much less in comparison with pIBV.

The hairpin hpS2 mimics stem 2 of pIBV (Figure 1(a)). The sequence in the single-stranded region is

Figure 4. Force-extension curves of pIBV-related hairpins. Five representative force-extension curves are shown in each panel for hpS1 (a) and hpS12 (c). For hpS2 (b), only one curve is shown to clearly show two distinct refolding patterns in the presence of Mg^{2+} (with a zip and without a zip). For hpS2, both Mg^{2+} and EDTA conditions show two distinct refolding patterns, one of which shows very slow refolding and often results in no recognizable zip. For hpS1 and hpS2, the red curve represents a theoretical curve for a double-stranded handle with fully folded pseudoknot conformation. As expected from the formation of a partially folded pseudoknot in the hpS1 and hpS2 constructs, their pulling curves were aligned well with a theoretical curve for the handles with a partially folded pseudoknot (the middle black curve). As for hpS12, the stack of five representative curves wasaligned with the theoretical curve based on the completely folded hairpin at low force regime and a completely unfolded hairpin (the addition of 38 nt in the single-stranded RNA sequence) at high force regime. For all curves, the pulling rate is 4–5 pN s^{-1}. The unfolding curves are in magenta, the refolding curves are in dark green. The number in parentheses is the total number of pulling curves used for calculating average unfolding and refolding forces.

very similar to the sequence of the corresponding nucleotides in pIBV but varies in the identity of four nucleotides in order to prevent hpS2 from forming a pseudoknot. The unfolding of hpS2 is a single rip of approximately 10 nm, consistent with disrupting the stem. The refolding behavior of hpS2 with its large loop is quite slow; on occasion there is no clear refolding rip (Figure 4(b)). This indicates that there is a dynamic equilibrium during refolding, which is to be expected in such a short stem. Like hpS1, the distribution of unfolding forces for hpS2 is much narrower than the distribution of pIBV and its unfolding force does not show appreciable dependence on the pulling rate. In the absence of Mg^{2+}, hpS2 unfolds at very low force (10–11 pN). Yet, its unfolding force increases significantly in the presence of Mg^{2+} (15–16 pN).

Overall, the unfolding and refolding characteristics of pIBV are drastically different from the hpS1 and hpS2 hairpins in the presence of Mg^{2+}. These results indicate that in Mg^{2+} the pIBV construct folds into a pseudoknot rather than partially folded conformations similar to hpS1 or hpS2.

The force-extension curves of hpS12: contributions of tertiary interactions

In order to further explore the contributions of tertiary interactions to RNA folding kinetics and thermodynamics we did a comparative study of the IBV pseudoknot and a hairpin (hpS12) containing the same base-pair sequence present in the two stems of the pseudoknot. Differences in the unfolding and refolding characteristics can be attributed to the presence of tertiary interactions that form the pIBV pseudoknot.

The hairpin hpS12 combines the nucleotide sequence of the pIBV stem 1 and stem 2 into one 17 base-pair stem with a tetraloop sequence of UUUU (Figure 1(a)). Just like pIBV, hpS12 shows one unfolding rip indicating the unfolding of the stem is a single step (Figure 4(c)). The average size of the hairpin unfolding transition is 15(±1.1) nm (Table 1). The unfolding forces of hpS12 fall in a narrow distribution around an average of 20 pN in the presence of Mg^{2+} at pulling rates from 10 pN s^{-1} to 2 pN s^{-1}. This is in great contrast to the broad distribution and higher average unfolding force of pIBV (26 pN at pulling rates at 2-3 pN s^{-1}; Table 1). However, in the absence of Mg^{2+}, both pIBV and hpS12 unfold at about the same force (17–18 pN at 3 pN s^{-1}).

Although the average unfolding force of pIBV slightly decreases at slower pulling rates, even at the slowest pulling rate (2–3 pN s^{-1}) in our study, pIBV unfolds at a higher force (26 pN) than hpS12 does (19 pN) in the presence of Mg^{2+}. Unlike pIBV, at moderately slow pulling rates (5 pN s^{-1} or slower), hpS12 displays a reversible transition in its unfolding and refolding processes, which is evidenced by the lack of hysteresis and appearance of "hopping" (Figure 4(c)). Although the presence of Mg^{2+} slightly increased hysteresis at a fast pulling rate (10 pN s^{-1}), hpS12 shows reversible unfolding and refolding both in Mg^{2+} and in EDTA. The ability of hpS12 to unfold and refold reversibly in the presence of Mg^{2+} indicates that Mg^{2+} does not slow its unfolding and refolding kinetics. This is in direct contrast with pIBV, which shows hysteresis in all conditions and significant hysteresis in the presence of Mg^{2+}. The hysteresis indicates that, in the presence of Mg^{2+}, the IBV pseudoknot conformation provides a stronger kinetic barrier to unfolding than its corresponding hairpin loop.

Overall, the general pattern of the force-extension curves of the IBV wild-type pseudoknot and its relevant hairpins indicate that pIBV requires the presence of Mg^{2+} to stabilize the pseudoknot conformation in our buffer conditions. The effect of Mg^{2+} on the unfolding characteristics of the tertiary structure pseudoknot is quite different from the effect of Mg^{2+} on the unfolding characteristics of a corresponding secondary structure, such as a hairpin.

Kinetics: pseudoknot *versus* hairpins

In order to quantify the differences in the kinetics of the tertiary structure pseudoknot and the secondary structure hairpin, rate coefficients (k) and distances to the transition states ($\Delta X^{\ddagger}$) were determined for the unfolding and refolding processes of pIBV and hpS12. Rates of reactions depend exponentially on force proportional to the distance to the transition state[45] as described by equation (1):

$$k = k_0 e^{F\Delta X^{\ddagger}/k_B T} \quad (1)$$

where k_0 is the apparent rate constant for unfolding at zero force, F is the force, k_B is the Boltzmann constant, and T is temperature in Kelvin. The value of k_0 is not the value that would actually be obtained at zero force, because $\Delta X^{\ddagger}$ is force dependent and approaches zero at zero force. Kinetic data can be obtained from the distribution of unfolding forces as a function of the rate at which the force is applied, the pulling rate. The relationship allows the force-dependent rate coefficients and distance to transition state values to be extracted from the distribution of unfolding forces using the following equation:[41,43]

$$\ln[r\ln(1/P)] = \ln[k_0/(\Delta X^{\ddagger}/k_B T)] + (\Delta X^{\ddagger}/k_B T)F \quad (2)$$

where r is pulling rate, P is the probability that a molecule is folded at force F and pulling rate r, and F is the force for unfolding. Analogous definitions apply when the equation is used to describe refolding. We have applied this method to obtain rate coefficients and distances to the transition state for the unfolding process of pIBV and hpS12 in both Mg^{2+} and EDTA conditions. The rate coefficients and distance to transition state values are shown in Table 2(A) and details of representative pIBV data are shown as an example in Figure 5.

The pIBV unfolding and refolding rate coefficients are not as dependent on force as the rate coefficients of hpS12. In the presence of Mg^{2+}, the

Table 2. The kinetic and thermodynamic characteristics of the force-extension curves of IBV pseudoknot (pIBV) and its related hairpins

A. *The unfolding and refolding kinetics of pIBV and its related hairpins*

	Unfolding						Refolding					
	Slope	*Y*-int	k_{1o} (0 pN)	k_1 (15 pN)	k_1 (20 pN)	$\Delta X_u^{\ddagger}$	Slope	*Y*-int	k_{-1o} (0 pN)	k_{-1} (15 pN)	k_{-1} (20 pN)	$\Delta X_r^{\ddagger}$
pIBV												
5 mM $MgCl_2$	0.314	−7.915	1.2×10^{-4}	0.013	0.061	1.4±0.3	−0.790	13.459	5.5×10^{5}	3.9	0.08	3.2±0.1
5 mM EDTA	1.536	−27.653	1.5×10^{-12}	0.015	33.0	6.2±0.4	−1.264	17.933	8.0×10^{7}	0.45	8.1×10^{-4}	5.6±0.8
hpS12												
5 mM $MgCl_2$	2.837	−52.442	4.8×10^{-23}	1.4×10^{-4}	210	11.5±0.9	−2.521	47.345	9×10^{20}	3.5×10^{4}	0.12	10.7±0.4
5 mM EDTA	2.963	−54.371	7.2×10^{-24}	1.5×10^{-4}	390	12.0±0.1	−2.606	49.504	8×10^{21}	8.7×10^{4}	0.19	11.0±1.5

k_1, rate constant for unfolding; ΔX_u, distance to transition state for unfolding (nm); Slope $= \Delta X^{\ddagger}/(k_BT)$

k_{-1}, rate constant for refolding; ΔX_r, distance to transition state for refolding (nm); *Y*-int $= \ln[k_0\Delta X^{\ddagger}/(k_BT)]$

B. *The free energy change* ΔG *at zero force* ($\Delta G0$) *during the unfolding and refolding processes of pIBV and its related hairpins (unit: kcal/mol)*

	pIBV	hpS12	hpS1	hpS2
5 mM $MgCl_2$	37±3	34±3	18±2	15±2
5 mM EDTA	27±2	30±3	14±2	9±2

pIBV unfolding rate coefficient undergoes approximately a fivefold change over a force range of 15 pN to 20 pN, (Table 2(A)) whereas the hpS12 rate coefficient of unfolding undergoes a 10^6-fold change over the same force range (Table 2(A)). Comparison between the refolding rate coefficients in the presence of Mg^{2+} shows that for pIBV the change is about 50-fold over the 15 pN to 20 pN range while for hpS12 the change is 10^5-fold over the same range (Table 2(A)).

The absence of Mg^{2+} increases the dependence of the pIBV rate coefficients on force, resulting in a 10^3-fold change in the unfolding rate coefficient and a 500-fold change in the refolding rate coefficient over the 15 pN to 20 pN range. For pIBV, the presence or absence of Mg^{2+} is seen to affect the unfolding rate much more than the refolding rate. For hpS12, the absence of Mg^{2+} does not result in a significant difference either in rates or in the dependence of the rates on the magnitude of external force. The unfolding and refolding rate coefficients of hpS12 show a very similar response to force in the absence of Mg^{2+} (10^6-fold change in unfolding and 5×10^5-fold change in refolding over 15 pN to 20 pN) compared with the response in the presence of Mg^{2+}.

The $\Delta X^{\ddagger}$ values for unfolding provide quantitative information about how the unfolding process depends on mechanical force. Molecules with a small distance to transition state for their unfolding processes are termed "brittle" and their unfolding rate constants are less influenced by external force. Molecules with larger $\Delta X^{\ddagger}$ values for their unfolding processes are termed "compliant" and their unfolding rate constants are more sensitive to the external force. For pIBV $\Delta X^{\ddagger}_{unfold}$ is about 1.3 nm in 5 mM Mg^{2+} and about 6.3 nm in 5 mM EDTA. The transition state is close to the initial folded state of the pseudoknot in Mg^{2+}, the pseudoknot is brittle. Moreover, Mg^{2+} slows the rate of unfolding near the unfolding force by at least a factor of 1000 (Table 2(A)). In the absence of Mg^{2+} the partially folded pseudoknot becomes compliant, and unfolds faster with a larger dependence on force.

In contrast to pIBV, hpS12 is compliant in both the presence and absence of Mg^{2+}. The distances to the transition states for both the unfolding and refolding processes of hpS12 are near 11-12 nm (Table 2(A)). For both molecules, the sum of $\Delta X^{\ddagger}_{unfold}$ and $\Delta X^{\ddagger}_{refold}$ is not equal to ΔX. For the pseudoknot the sum of distances to transition states is less than the size of the transition and for the hairpin the sum is greater than the size of the transition. The hairpin data are consistent with a previous study on the mechanical unfolding of an RNA hairpin where the $\Delta X^{\ddagger}_{unfold}$ and $\Delta X^{\ddagger}_{refold}$ values were both approximately 12 nm and the total ΔX was approximately 18 nm.[41] The discrepancies between the sums $\Delta X^{\ddagger}_{unfold}$ and $\Delta X^{\ddagger}_{refold}$ and the total ΔX indicate that the unfolding processes are not the reverse of the refolding processes. This is understandable when one considers that transition states of the forward and reverse reactions are identical only for two-state reactions. In the case of RNA folding reactions studied here, the reactions are two-state in the scale of seconds. However, many RNA folding reactions have intermediates in the millisecond or microsecond time scale[53] and, therefore, the forward and reverse reactions are not necessarily identical.

Thermodynamics: pseudoknot *versus* hairpins

We also investigated the effect of Mg^{2+} on the thermodynamic stability of the pIBV and its related hairpins. We could not directly measure the reversible work for the unfolding and refolding processes of pIBV in both the presence and the absence of Mg^{2+}, since the processes are irreversible even at our

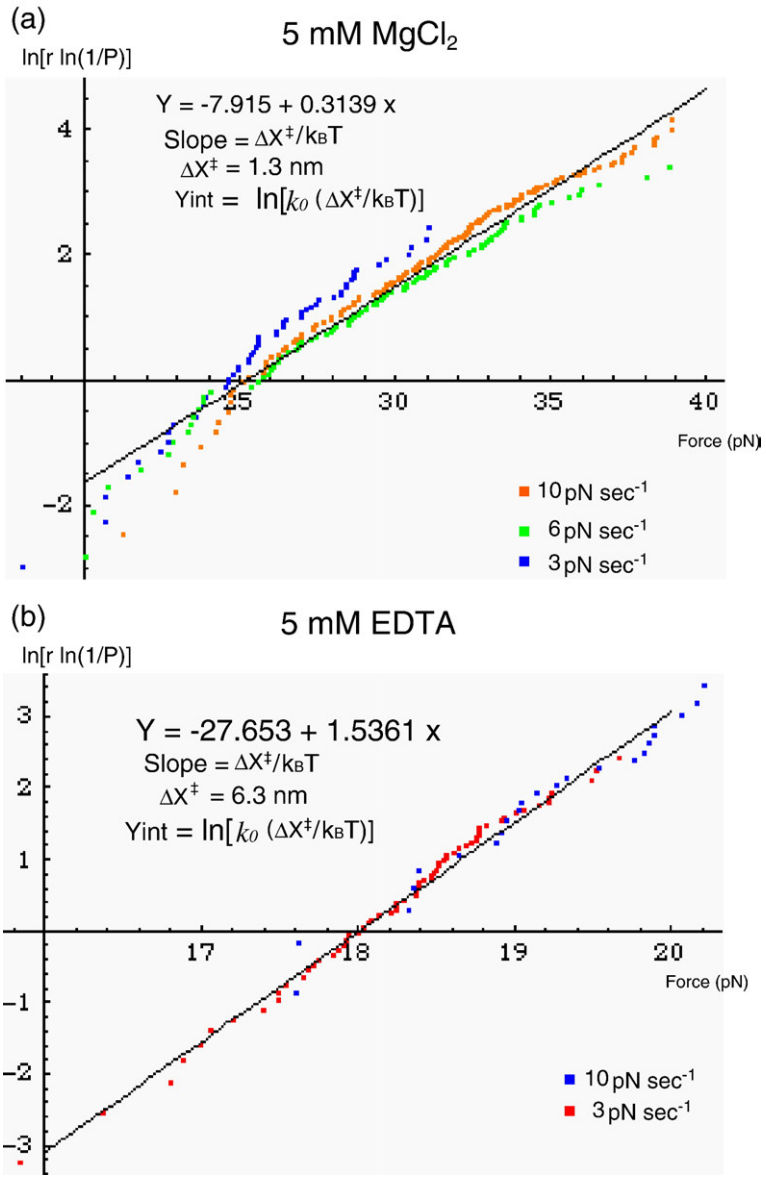

Figure 5. Kinetic analysis of the force-extension curves of pIBV. The plots of unfolding forces *versus* ln *[r* ln*(1/P)]* are shown at three different pulling rates in Mg^{+2} (a) and at two different pulling rates in EDTA (b). Here r is the pulling rate, P is the probability that a molecule is folded at force F. The data with different pulling rates fit reasonably well with a single slope. The distance to the transition state ($\Delta X^{\ddagger}$) was calculated from the slope of the plot ($\Delta X^{\ddagger}/(k_BT)$) while the apparent rate constant at zero force (k_0) was calculated from the Y-intercept = ln $[k_0/(\Delta X^{\ddagger}/(k_BT))]$.

slowest pulling rates. However, using the Crook's fluctuation theorem we could estimate the reversible work from many repeated irreversible unfolding and refolding pulling curves[54] (Figure 6). The reversible work is equal to the Gibbs free energy change of a molecule during the transition between its folded and unfolded state. We pulled RNA molecules many times (~70 pulling curves) using the same experimental setting on the same day to obtain the distributions of their unfolding and refolding work. Though these are irreversible processes, using the Crook's fluctuation theorem,[55] we obtained the reversible unfolding/refolding work (ΔG) from the crossover point of the unfolding and refolding work distributions. Using this method, we found that the estimated reversible unfolding work of pIBV drastically increased in the presence of Mg^{2+} (63(±1) kcal mol^{-1} at an unfolding force of 29 pN) compared with the value in the absence of Mg^{2+} (45(±1) kcal mol^{-1} at an unfolding force of 18 pN), which indicates that the presence of Mg^{2+} significantly stabilizes the pseudoknot (Figure 6 and Table 2(B)). Therefore, the binding of Mg^{2+} not only affects the kinetics, but also the thermodynamics of the unfolding process of the IBV pseudoknot.

Since mechanical unfolding of hpS12 can be done reversibly at reasonably slow pulling rates, we could directly obtain the reversible unfolding work (ΔG) by measuring the area under the rip at the unfolding force. The reversible unfolding work of hpS12 at an unfolding force of 20 pN is similar both in the presence of Mg^{2+} (5 mM $MgCl_2$, 51(±2) kcal mol^{-1}) and in the absence of Mg^{2+} (5 mM EDTA, 46(±2) kcal mol^{-1}). This result is quite different from pIBV for which Mg^{2+} appreciably stabilizes its folded conformation.

The free energy change at zero force for the unfolding and refolding process is also informative. The free energy at zero force is obtained by subtracting the free energy of stretching the single strand to the unfolding force[45,56] As shown in Table 2(B), the free energy changes calculated in this way are in a reasonable range compared with the estimated free energy using the RNA folding program

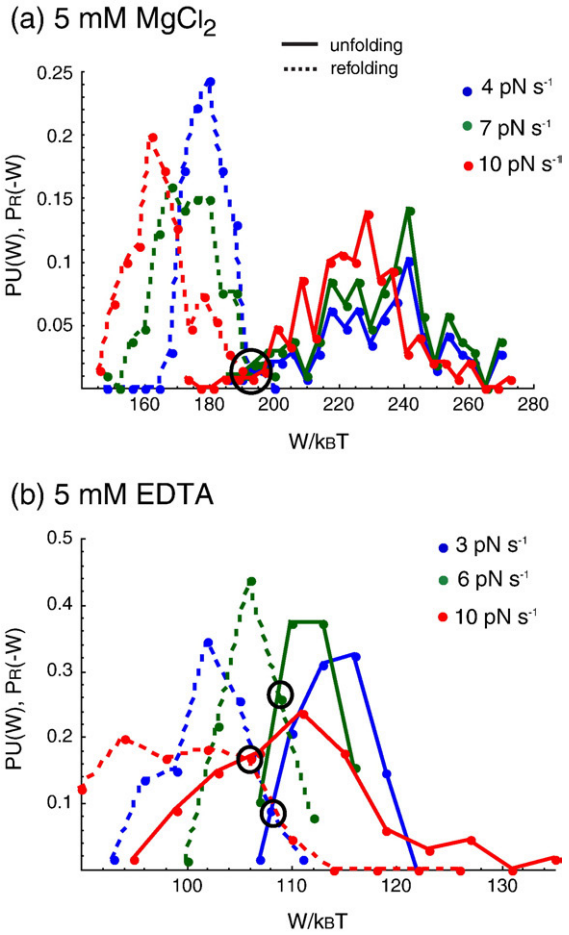

Figure 6. Estimated reversible work of pIBV using Crook's fluctuation theorem. The probability distributions of the work, W, for the unfolding (continuous lines) and refolding (broken lines) of pIBV in Mg^{2+} (a) and EDTA (b). Negative work, $P_R(-W)$ were plotted for refolding. Statistics: For Mg^{2+}, 148 curves, three molecules ($r=4$ pNs^{-1}), 152 curves, two molecules ($r=10$ pNs^{-1}). For EDTA, 68 curves, one molecule ($r=3$ pNs^{-1}), 78 curves, one molecule ($r=6$ pNs^{-1}), 68 curves, one molecule ($r=10$ pNs^{-1}). Work values were binned into eight to 12 equally spaced intervals. Unfolding and refolding distributions at different pulling rates show similar crossing points (circled in black) that reasonably match with one another (194(±2.1) k_BT for Mg^{2+}, 108(±1.5) k_BT for EDTA).

Mfold[26] based on the Turner rules[57,58] (36.7 kcal mol^{-1}, in 1 M NaCl at 21 °C).

The IBV pseudoknot in comparison with three mutant pseudoknots

In order to gain insight into the mechanism of −1 programmed ribosomal frameshifting, the mechanical unfolding and refolding of the wild-type IBV pseudoknot and its three mutant pseudoknots were characterized using constant force experiments. All experiments were done using folding and unfolding forces ranging from 19pN–24 pN and a pH 7.5 buffer containing 20 mM Tris, 50 mM KCl, 5 mM $MgCl_2$.

Constant force experiments are of two types, hopping and force-jump. During hopping experiments, an RNA molecule is held at a constant force at which both unfolding and refolding transitions can be observed in an experimentally accessible time scale.[41,42,51] However, hopping experiments can only access forces near the equilibrium; for many molecules the range of forces is too narrow for the collection of data across a significant range of forces. To perform constant force experiments across a wider range of forces the force-jump method can be used instead. A diagram of a force-jump experiment is shown in Figure 7. The cycle begins at low force with the molecule in its folded conformation. Next, the force is rapidly increased to a value at which the molecule will unfold within an experimentally accessible time scale. Simultaneously, the stretching of the RNA/DNA hybrid handles resulting from the sudden force increase produces an increase in extension (ΔX) of the molecular tether. The new imposed force is held constant until an increase in extension due to the unfolding of the molecule occurs. Once unfolding has been observed, force is ramped higher to ensure that complete unfolding of the molecule has indeed occurred. After this second force increase, a gradual increase in extension occurs because of further stretching of the handles. Next the force is rapidly decreased to a value at which the molecule will refold on an experimentally accessible time scale and finally ramped to a lower value to ensure complete refolding of the molecule before the cycle is repeated.[51]

Data from constant force experiments are represented by plots of extension *versus* time (Figure 8). The measured sizes of the folded to unfolded transitions at 21–24 pN force are in the range of 10 nm–15 nm (for details, see Table 3). Based on the known structures of other pseudoknots[59–61] we estimate that the 3′ to 5′ distances of the folded pseudoknots to be approximately: 6(±1) nm. The lengths of single-stranded RNA were calculated

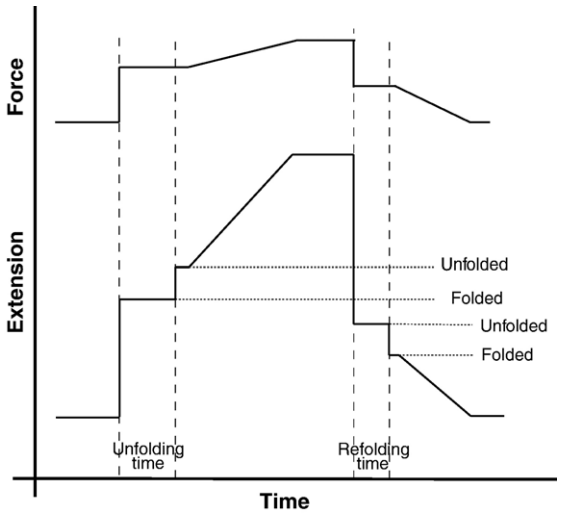

Figure 7. Diagram of a force-jump experiment. The changes in force and extension over time during a force-jump experiment are shown schematically.

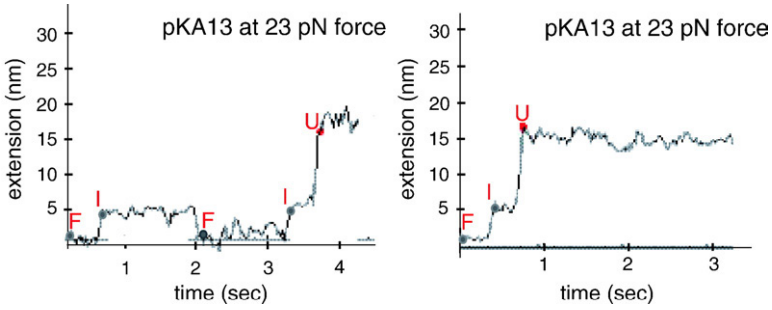

Figure 8. Force-jump traces of pKA13 unfolding showing intermediates. Extension *versus* time plots of data taken from force-jump experiments done with an unfolding force of 23 pN in a pH 7.5 buffer containing pH 20 mM Tris, 50 mM KCl, 5 mM $MgCl^2$. At time zero, the molecule is in the folded conformation (F) and extension is constant until unfolding or partial unfolding of the pseudoknot produces the sharp increase in extension. The smaller increases in extension are attributed to partial unfolding to an intermediate state (I), and the larger increases are attributed to a transition from the intermediate state to the fully unfolded state (U).

from the WLC model. In the 21pN–24 pN force range, the conversion factor is 0.46 nm per nucleotide and leads to calculated changes in extension of: 11–14 nm (Table 3), which are in reasonable agreement with the measured changes in extension.

The two-stem structure of pseudoknots suggests the possible existence of partially folded intermediate states containing one of the constituent hairpins. For pIBV, the data from force ramp as well as constant force experiments give no evidence of detectable intermediates, indicating a single-step transition between a folded state and unfolded state. However, as shown in Figure 8, an IBV mutant pseudoknot, pKA13, infrequently (about 10% of the trajectories in the 23 pN–25 pN unfolding force and 21 pN–23 pN refolding force range) shows two-step unfolding/refolding processes revealing the presence of a distinct intermediate in the constant-force experiments. This observation is consistent with the observation of two-step transitions in the force-extension curves of pKA13 at slow pulling rates (data not shown). These results indicate that pKA13 goes through a detectable, partially folded intermediate state during its unfolding and refolding. Evidence of intermediate states was present, but less frequent in pKA18 data and rare in pKA9 data. The molecular explanation for this difference in the folding pathways of the four pseudoknots is unclear. We report the observation of these intermediates without speculation on their significance, and with hopes that it may prove useful to future work on RNA folding. Though the presence of intermediates was observed, to a varying degree, in the three mutant pseudoknots, overall a one-step transition without intermediate states is the most dominant transition pattern for all three IBV mutant pseudoknots.

Table 3. Extension and change in extension values for the four pseudoknots

	Folded to unfolded		Intermediate	
	Transitions (nm)		Transitions (nm)	
	Estimated ΔX	Measured ΔX F to U	Measured ΔX F to I	Measured ΔX I to U
pIBV	14	15±2	N/A	N/A
pKA18	13	14±1	5±2	10±2
pKA13	12	12±2	5±1	10±1
pKA9	11	10±1	5±1	9±1

Estimated ΔX, theoretical change in extension based on estimated 3′ to 5′ distance of the folded conformation and final extension values calculated from the WLC model for a force range 21 pN–24 pN.
Measured ΔX, measured change in extension values determined at 24 pN, 20 mM Tris (pH 7.5), 50 mM KCl and 5 mM $MgCl_2$.
ΔX F to U values are for the transition from fully folded to fully unfolded.
ΔX F to I values are for the transition from fully folded to partially folded.
ΔX I to U values are for the transition from partially folded to fully unfolded.

Kinetics: wild-type *versus* mutant pseudoknots

Analysis of the kinetics of mechanical folding and unfolding of the pseudoknots was done assuming that the folding and unfolding transitions can be considered as a two-state transition. To minimize the occurrence of non-two state behavior, our analysis includes only unfolding data taken at an unfolding force of 23 pN or higher, and refolding data taken at a refolding force of 23 pN or lower for the pKA13 and pKA18. This force range can accurately characterize the folding reactions and in fact is greater than or equal to the force range used in previously published characterization of the mechanical unfolding of RNA.[41,51,62,63] Our assumption is validated by the results showing that the distributions of the lifetimes of folded or unfolded states of these mutants during constant force experiments are well fit to single-exponential first-order kinetics.

The lifetimes (τ) of the folded and unfolded states were directly measured from constant force experiments. The unfolding or refolding rate (k_1 or k_{-1}) at a particular force is inversely related to the average life time of the folded or unfolded state, $<\tau>$, at that force:[51]

$$k_1 = 1/<\tau_{\text{unfolding}}> \; k_{-1} = 1/<\tau_{\text{refolding}}> \qquad (3)$$

Distributions of the lifetimes at a constant force are well fit to a single exponential, consistent with first-order kinetics for the process as shown in equation (4):

$$P = \exp(-k_F t) \qquad (4)$$

where P is the probability that a molecule is still folded, k_F is the rate constant at force F and t is time.[45]

The equilibrium constant (K_{eq}) of a reaction is equal to the ratio of the forward and reverse rate constants:

$$K_{eq} = k_1/k_{-1} \quad (5)$$

Rate constants for the unfolding and the refolding processes (as determined by the reciprocal of the average lifetimes) and the equilibrium constants derived from those rate constants, are listed in Table 4. Interestingly, in a narrow force range (23.5 pN–24.5 pN), unfolding rate constants of pIBV and its mutants shows noticeable correlation to their frameshifting efficiencies. As shown in Table 4, at forces near 24 pN, pseudoknots with higher frameshifting efficiency showed slower unfolding rates.

The force dependence of the rate coefficients is exponentially dependent on the distance to the transition state as described by equation (1).[45] Distances to transition states were determined by plotting the natural log of the rate coefficients *versus* force (Figure 9). The $\Delta X^{\ddagger}$ values for unfolding processes, $\Delta X^{\ddagger}_{unfold}$, were found to be: 2(±0.5) nm for pIBV; 6(±1) nm for pKA18; 4(±1) nm for pKA13; and 3(±1) nm for pKA9. The $\Delta X^{\ddagger}$ values of refolding processes ($\Delta X^{\ddagger}_{refold}$) were: 5(±1) nm for pIBV; 4(±2) nm for pKA18; 3(±1) nm for pKA13; and 2(±1) nm for pKA9. For all four pseudoknots, the sum of $\Delta X^{\ddagger}_{unfold} + \Delta X^{\ddagger}_{refold}$ do not equal the total change in extension. As discussed above, this discrepancy indicates that the refolding process is not the reversal of the unfolding process.

Thermodynamics: wild-type *versus* mutant pseudoknots

The change of free energy values of the folding and unfolding processes of the pseudoknots were measured using the rate constants determined from the constant-force experiments. When the natural log of the rate constant is plotted against force, the unfolding and refolding lines cross at the critical force (F_C) where the unfolding and refolding rate constants are equal, and thus the equilibrium constant is equal to 1. We can then obtain the change of free energy (ΔG) from the following equation:

$$\Delta G_{FC} = (F_C)(\Delta X) \quad (6)$$

where ΔG_{FC} is the change in free energy at F_C. To allow comparison between the thermodynamics of different RNA molecules and comparison with bulk experiments at zero force, ΔG_{FC} values need to be converted to the change in free energy at zero force (ΔG_0) by subtracting the free energy due to stretching of the RNA.[45,56] The ΔG_0 values were found to be: 31(±4) kcal mol^{-1} for pIBV; 34(±3) kcal mol^{-1} for pKA18; 32(±3) kcal mol^{-1} for pKA13; and 19(±4) kcal mol^{-1} for pKA9 (Table 5).

The change in free energy for the RNA folding can be calculated using the Mfold program and nearest-neighbor free energy parameters.[26,58] Though Mfold does not treat tertiary structure, the thermodynamic contributions of individual RNA structural elements can be used to estimate the thermodynamic stability of an RNA molecule with tertiary structure. Specifically, the stability of a pseudoknot can be approximated from the free energy parameters by adding the contributions of the base-paired stems and subtracting the entropic penalty created by the loops. Values for ΔG_0 (at 21 °C and 1 M NaCl) were calculated in this way for the four pseudoknots and are shown in Table 5.

Discussion

The contributions of tertiary interactions in RNA conformation

Here, we investigated the mechanical characteristics of the IBV pseudoknot in comparison with its related hairpins in order to gain insight into the contributions of tertiary interactions to RNA folding kinetics and thermodynamics. The most significant differences between the RNA pseudoknot and the corresponding RNA hairpins were: (1) Mg^{2+} is crucial to the tertiary interactions that stabilize the pseudoknot conformation, but has minimal effect on the hairpins; (2) the pseudoknot requires higher

Table 4. Rate constants of unfolding (k_1) and refolding (k_{-1}) for the pseudoknots at various forces

		Force			
		22 pN	23 pN	24 pN	25 pN
pIBV	k_1 (s^{-1})	***0.07*±*0.01***	***0.14*±*0.02***	***0.25*±*0.04***	0.37±0.06
	k_{-1} (s^{-1})	$5.0\times10^{-3}\pm6.6\times10^{-4}$	$3.8\times10^{-4}\pm5.3\times10^{-5}$	$1.0\times10^{-4}\pm1.4\times10^{-5}$	$2.8\times10^{-5}\pm3.9\times10^{-6}$
pKA18	k_1 (s^{-1})	$0.01\pm1.5\times10^{-3}$	***0.06***$\pm9.0\times10^{-3}$	***0.17*±*0.03***	***0.86*±*0.13***
	k_{-1} (s^{-1})	***0.64*±*0.25***	***0.16*±*0.06***	0.08±***0.03***	0.03±***0.01***
pKA13	k_1 (s^{-1})	$0.05\pm9.5\times10^{-3}$	***0.12*±*0.02***	***0.44*±*0.08***	***0.82*±*0.15***
	k_{-1} (s^{-1})	***0.82*±*0.33***	***0.24*±*0.09***	0.13±***0.05***	0.06±***0.02***
pKA9	k_1 (s^{-1})	***0.22*±*0.03***	***0.50*±*0.08***	1.04±***0.16***	2.04±***0.31***
	k_{-1} (s^{-1})	***0.69*±*0.22***	***0.27*±*0.09***	0.17±***0.05***	0.10±***0.03***

Values shown in regular font were determined experimentally.
Values shown in bold italic font were extrapolated from experimental values.
Extrapolated values were calculated from the linear fit of a plot of the natural log of rate constants *versus* force (Figure 8).

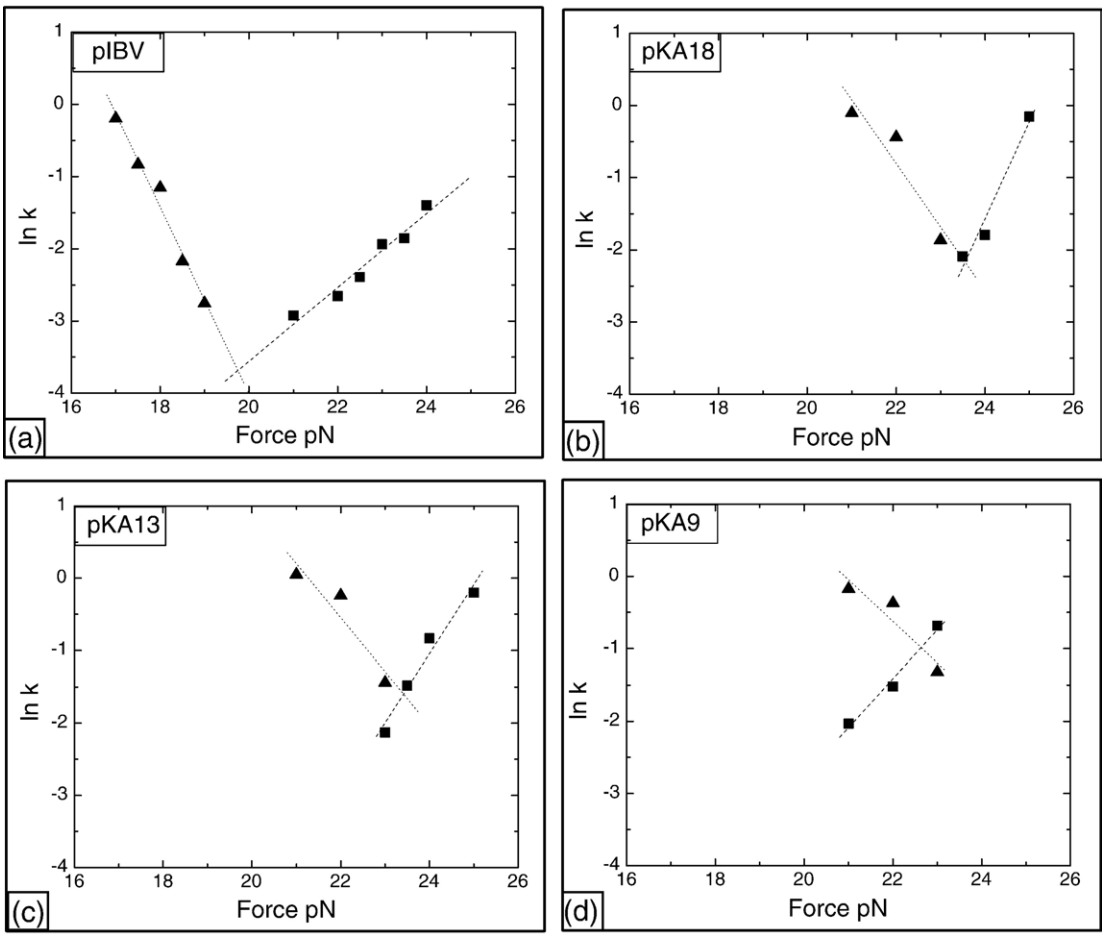

		$\ln k = F(\Delta X^{\ddagger}/k_B T) + \ln k_0$	$\Delta X^{\ddagger}$
pIBV	unfold	ln k= F(0.51) -13.80	2.1 ± 0.5 nm
	refold	ln k = F(-1.29) + 21.84	5.3 ± 0.7 nm
pKA18	unfold	ln k = F(1.31) - 33.76	5.5 ± 0.8 nm
	refold	ln k = F(-0.88) + 18.57	3.6 ± 1.6 nm
pKA13	unfold	ln k = F(0.96) - 23.95	3.9 ± 1.2 nm
	refold	ln k = F(-0.75)) + 15.88	3.1 ± 1.1 nm
pKA9	unfold	ln k = F(0.68) - 16.26	2.8 ± 0.5 nm
	refold	ln k = F(-0.57) + 12.00	2.4 ± 0.7 nm

Figure 9. Natural log of rate constants *versus* unfolding and refolding force. Natural log of the rate constants for unfolding (■) and refolding (▲) plotted against force for pIBV (a), pKA18 (b), pKA13 (c) and pKA9 (d). The linear fits of the unfolding data (dotted lines) and of the refolding data (broken lines) intersect at the critical force. The lines are described by equation (6): $\ln k = F(\Delta X^{\ddagger}/k_B T) + \ln k_0$ where k is the rate constant, F is the force, $\Delta X^{\ddagger}$ is the distance to transition state, k_B is the Boltzmann constant, T is the temperature and k_0 is the apparent rate constant at zero force. Values for $\Delta X^{\ddagger}$ obtained from these equations are listed for the unfolding and refolding transitions of the four pseudoknots. Data were obtained in pH 7.5 buffer containing 20 mM Tris, 50 mM KCl and 5 mM $MgCl_2$.

force to unfold than the hairpin with the same base-pairs; (3) the thermodynamic stabilities of the pseudoknot and hairpin are similar, but the kinetics of unfolding is much slower for the pseudoknot.

The thermodynamic stability of the hairpin hpS12 predicted by Mfold[26,58] is 37 kcal mol^{-1} in 1 M NaCl at 21 °C. The calculated thermodynamic stability of pIBV (as described above) was 35 kcal mol^{-1}. As pIBV and hpS12 have the same base-pairs (Figure 1), we expect them to have similar calculated thermal stabilities. Our force-ramp data (in 20 mM Tris, 50 mM NaCl, 5 mM $MgCl_2$) give the free energy change at zero force, ΔG_0, of 37(±3) kcal mol^{-1} for the unfolding of pIBV and 34(±3) kcal mol^{-1} for the unfolding of hpS12. These results are consistent with our expectations. However, in the presence of Mg^{2+}, the average unfolding force of pIBV is significantly higher than that of hpS12 at all pulling rates (Table 1). The mechanical unfolding of pIBV is a kinetically controlled process, except at extremely

Table 5. Change in free energy values for the four pseudoknots

	Change in free energy		
	Experimental ($F = Fc$) (kcal mol^{-1})	Extrapolated ($F = 0$ pN) (kcal mol^{-1})	Theoretical ($F = 0$ pN) (kcal mol^{-1})
pIBV	42	31	35
pKA18	47	34	43
pKA13	45	32	40
pKA9	31	19	34

Experimental: determined from the critical force and change in extension at that force.
Extrapolated: determined from the experimental values by subtracting the free energy needed to stretch the molecule to the critical force.
Calculated: determined from the Turner free energy values for stacking energies and destabilization by loops.

slow pulling rates where the process is reversible. Thus, although the thermodynamic stability of a the tertiary structure-forming pIBV can be similar to its secondary structure counterpart (hpS12), its response to mechanical force, and in particular the kinetics of this response is very different to the corresponding hairpin.

Indeed, the unfolding kinetics of the pseudoknot (pIBV) is not only much slower than that of the hairpin (hpS12), but the force dependence of its rate of unfolding is also much smaller. The pseudoknot is brittle (short distance from its folded state to its transition state), whereas the secondary structure is compliant (larger distance from its folded state to its transition state). The short distance to the transition state characterizes the fact that the pseudoknot unfolds over a wide range of forces. The standard deviation of the average unfolding force distribution is noticeably larger for pIBV than it is for the corresponding hairpin; the unfolding rate coefficient of pIBV also changes much more slowly with a change in the unfolding force compared with hpS12. The distance to the transition state of hpS12 for both unfolding and refolding is large (~12 nm), which is consistent with earlier studies of RNA hairpins.[41]

Minus-1 programmed ribosomal frameshifting

Our data clearly show that the tertiary structure pseudoknot has unique mechanical characteristics compared to the secondary structure hairpin. Pseudoknots unfold at higher forces than hairpins, and their rates of unfolding increase much less with increasing force. Do these characteristics provide insight into the role of pseudoknots in –1 programmed ribosomal frameshifting? Yes. We propose that the slow unfolding of a pseudoknot compared to a hairpin, even as the ribosome applies increasing force, favors frameshifting. Do the characteristics of the mechanical unfolding of the mutant pseudoknots explain their relative frameshifting efficiency? No. We found no general correlation between mechanical properties, such as distance to the transition state for unfolding, and the variation in frameshifting efficiency (2%–46%). Chemical properties not mirrored in the mechanical characteristics must also be important. We did see that near 24 pN the frequency with which the pseudoknots induce frameshifting is inversely proportional to their rate constants of unfolding (Table 4). Though the correlation is only present over a very narrow range of forces it may prove to have some significance once the mechanochemistry of the ribosome is characterized.

Conclusion

We show that Mg^{2+} significantly contributes to the formation of a unique tertiary conformation of IBV pseudoknot, which shows quite different mechanical properties compared with its corresponding hairpin. The unique kinetic behavior of the IBV wild type pseudoknot suggests its biological function in the frameshifting process may be caused by its role as a kinetic barrier against the unfolding machinery of a ribosome during translation. Though mutant pseudoknots do not show general correlation between their kinetic behavior and their frameshifting efficiency, we do observe correlation with their unfolding rates in a specific range of unfolding forces.

Methods and Materials

RNA molecules were prepared as optical tweezer constructs as described.[41,42,64] Commercially synthesized DNA oligonucleotides (Operon) corresponding to the RNA sequences studied here were inserted into the vector pBR322 (New England Biolabs) between the EcoRI and HindIII sites, creating a plasmid that was used to transform competent BL21 *Escherichia coli* cells (Invitrogen). The plasmid was replicated by the bacteria and a DNA template for RNA transcription was removed from the plasmid by enzymatic digestion resulting in a template corresponding to the RNA sequence of the appropriate molecule plus approximately 500 DNA base-pairs on each side that correspond to the RNA sequence of the handle regions. The template was recovered by miniprep (Qiagen) and sequenced by the University of California Berkeley (UCB) sequencing facility. The DNA template was amplified by the polymerase chain reaction (PCR) containing a T7 promoter sequence at the 5′ end, and sequenced by the UCB sequencing facility. RNA molecules were transcribed from the DNA templates by bacteriophage T7 RNA polymerase (Ambion). The RNA was prepared as an optical tweezers construct by annealing the DNA handles to the single-stranded RNA handle regions. DNA handle A (pBR322 bases 3821 to 3) was amplified by PCR and then biotinylated at the 3′ end using an exchange reaction by T4 DNA polymerase. The downstream primer used for PCR amplification of DNA handle B (pBR322 bases 30 to 628) was modified to have a terminal digoxigenin group. The biotin and digoxigenin allowed the RNA–DNA handles flanking the RNA sequence to be attached to a streptavidin coated polystyrene bead (Spherotech) and an anti-digoxigenin coated polystyrene bead (Spherotech).

All experiments were performed on a dual-beam optical tweezers instrument[65] in an ambient temperature of 20–22 °C. Force-ramp experiments were performed in either magnesium buffer (20 mM Tris, 50 mM NaCl, 5 mM $MgCl_2$ (pH 7.5)) or EDTA buffer (20 mM Tris, 50 mM KCl, 0.5 mM EDTA (pH 7.5)). RNA constructs were pulled at forces ranging between 2 pN and 35 pN at loading rates of 2 pN s^{-1} to 20 pN s^{-1}. Constant force experiments were performed in 20 mM Tris, 50 mM KCl, 5 mM $MgCl_2$ (pH 7.5). RNA constructs were subjected to forces of 3 pN–40 pN, with incubation forces (forces used to observe unfolding and/or refolding) of 17 pN–26 pN. Constant force data were collected at 100–200 Hz.

All experiments positioned the RNA constructs in the optical tweezers in the following manner. Streptavidin-coated beads of approximately 2 μm were added to a microfluidic chamber filled with the appropriate buffer. A streptavidin bead was caught in the laser trap and then transferred to a micropipette attached to a piezoelectric stage. The RNA constructs were incubated with anti-digoxigenin coated beads of approximately 3 μm in the same buffer and then added to the microfluidic chamber. An anti-digoxigenin bead was caught in the laser trap and the streptavidin micropipette bead was moved near the anti-digoxigenin trap bead. The micropipette bead repeatedly approached the trap bead until a biotin-streptavidin connection was made, resulting in an RNA tether holding both beads together. Force was exerted on the molecule by moving the micropipette relative to the laser trap. The force on the bead in the trap, and therefore the force on the molecule held between the two beads, was determined from the change in the momentum of the laser light as it passed through the trap.[65] The change in extension of the RNA was measured from the change in position of the beads.[65]

Acknowledgements

The authors are grateful for the technical help and valuable discussions from Dr Steven B. Smith, Dr Pan Li and Dr Delphine Collin. This work was supported by grants from National Institutes of Health (MBRS-SCORE GM48135) and National Science Foundation (MCB-0417248) (to C.-H. K.) and National Institutes of Health grant GM10840 (to I.T.).

References

1. Pleij, C. W. A. (1994). RNA Pseudoknots. *Curr. Opin. Struct. Biol.* **4**, 337–344.
2. Feng, Y. X., Yuan, H., Rein, A. & Levin, J. G. (1992). Bipartite signal for read-through suppression in murine leukemia virus mRNA: an eight-nucleotide purine-rich sequence immediately downstream of the gag termination codon followed by an RNA pseudoknot. *J. Virol.* **66**, 5127–5132.
3. Powers, T. & Noller, H. F. (1991). A functional pseudoknot in 16S ribosomal RNA. *EMBO J.* **10**, 2203–2214.
4. Nameki, N., Felden, B., Atkins, J. F., Gesteland, R. F., Himeno, H. & Muto, A. (1999). Functional and structural analysis of a pseudoknot upstream of the tag-encoded sequence in *E. coli* tmRNA. *J. Mol. Biol.* **286**, 733–744.
5. Ferre-D'Amare, A. R., Zhou, K. & Doudna, J. A. (1998). Crystal structure of a hepatitis delta virus ribozyme. *Nature*, **395**, 567–574.
6. Jabri, E., Aigner, S. & Cech, T. R. (1997). Kinetic and secondary structure analysis of *Naegleria andersoni* GIR1, a group I ribozyme whose putative biological function is site-specific hydrolysis. *Biochemistry*, **36**, 16345–16354.
7. ten Dam, E., Pleij, K. & Draper, D. (1992). Structural and functional aspects of RNA pseudoknots. *Biochemistry*, **31**, 11665–11676.
8. Gilley, D. & Blackburn, E. H. (1999). The telomerase RNA pseudoknot is critical for the stable assembly of a catalytically active ribonucleoprotein. *Proc. Natl Acad. Sci. USA*, **96**, 6621–6665.
9. Tzfati, Y., Knight, Z., Roy, J. & Blackburn, E. H. (2003). A novel pseudoknot element is essential for the action of a yeast telomerase. *Genes Dev.* **17**, 1779–1788.
10. Wilkinson, S. R. & Been, M. D. (2005). A pseudoknot in the 3′ non-core region of the glmS ribozyme enhances self-cleavage activity. *RNA*, **11**, 1788–1794.
11. Nishikawa, F. & Nishikawa, S. (2000). Requirement for canonical base pairing in the short pseudoknot structure of genomic hepatitis delta virus ribozyme. *Nucl. Acids Res.* **28**, 925–931.
12. Wadkins, T. S., Perrotta, A. T., Ferre-D'Amare, A. R., Doudna, J. A. & Been, M. D. (1999). A nested double pseudoknot is required for self-cleavage activity of both the genomic and antigenomic hepatitis delta virus ribozymes. *RNA*, **5**, 720–727.
13. Deschenes, P., Ouellet, J., Perreault, J. & Perreault, J. P. (2003). Formation of the P1.1 pseudoknot is critical for both the cleavage activity and substrate specificity of an antigenomic trans-acting hepatitis delta ribozyme. *Nucl. Acids Res.* **31**, 2087–2096.
14. Pfingsten, J. S., Costantino, D. A. & Kieft, J. S. (2006). Structural basis for ribosome recruitment and manipulation by a viral IRES RNA. *Science*, **314**, 1450–1454.
15. Wang, C., Le, S. Y., Ali, N. & Siddiqui, A. (1995). An RNA pseudoknot is an essential structural element of the internal ribosome entry site located within the hepatitis C virus 5′ non-coding region. *RNA*, **1**, 526–537.
16. Serganov, A., Ennifar, E., Portier, C., Ehresmann, B. & Ehresmann, C. (2002). Do mRNA and rRNA binding sites of *E.coli* ribosomal protein S15 share common structural determinants? *J. Mol. Biol.* **320**, 963–978.
17. Ringquist, S., Jones, T., Snyder, E. E., Gibson, T., Boni, I. & Gold, L. (1995). High-affinity RNA ligands to *Escherichia coli* ribosomes and ribosomal protein S1: comparison of natural and unnatural binding sites. *Biochemistry*, **34**, 3640–3648.
18. Philippe, C., Eyermann, F., Benard, L., Portier, C., Ehresmann, B. & Ehresmann, C. (1993). Ribosomal protein S15 from *Escherichia coli* modulates its own translation by trapping the ribosome on the mRNA initiation loading site. *Proc. Natl Acad. Sci. USA*, **90**, 4394–4398.
19. Baranov, P. V., Gesteland, R. F. & Atkins, J. F. (2002). Recoding: translational bifurcations in gene expression. *Gene*, **286**, 187–201.
20. Farabaugh, P. J. (2000). Translational frameshifting: implications for the mechanism of translational frame maintenance. *Prog. Nucl. Acid Res. Mol. Biol.* **64**, 131–170.
21. Brierley, I. & Pennell, S. (2001). Structure and function of the stimulatory RNAs involved in programmed eukaryotic-1 ribosomal frameshifting. *Cold Spring Harbor Symp. Quant. Biol.* **66**, 233–248.

22. Wills, N. M., Gesteland, R. F. & Atkins, J. F. (1991). Evidence that a downstream pseudoknot is required for translational read-through of the Moloney murine leukemia virus gag stop codon. *Proc. Natl Acad. Sci. USA*, **88**, 6991–6995.
23. Giedroc, D. P., Theimer, C. A. & Nixon, P. L. (2000). Structure, stability and function of RNA pseudoknots involved in stimulating ribosomal frameshifting. *J. Mol. Biol.* **298**, 167–185.
24. Alam, S. L., Atkins, J. F. & Gesteland, R. F. (1999). Programmed ribosomal frameshifting: much ado about knotting! *Proc. Natl Acad. Sci. USA*, **96**, 14177–14179.
25. Mathews, D. H. & Turner, D. H. (2006). Prediction of RNA secondary structure by free energy minimization. *Curr. Opin. Struct. Biol.* **16**, 270–278.
26. Zuker, M. (2003). Mfold web server for nucleic acid folding and hybridization prediction. *Nucl. Acids Res.* **31**, 3406–3415.
27. Bustamante, C. (2004). Of torques, forces, and protein machines. *Protein Sci.* **13**, 3061–3065.
28. Walter, A. E. & Turner, D. H. (1994). Sequence dependence of stability for coaxial stacking of RNA helixes with Watson-Crick base paired interfaces. *Biochemistry*, **33**, 12715–12719.
29. Draper, D. E. (1996). Strategies for RNA folding. *Trends Biochem. Sci.* **21**, 145–149.
30. Brion, P. & Westhof, E. (1997). Hierarchy and dynamics of RNA folding. *Annu. Rev. Biophys. Biomol. Struct.* **26**, 113–137.
31. Vinod, K. & Misra, D. E. D. (1998). On the role of magnesium ions in RNA stability. *Biopolymers*, **48**, 113–135.
32. Pan, T. & Sosnick, T. (2006). RNA Folding during transcription. *Annu. Rev. Biophys. Biomol. Struct.* **35**, 161–175.
33. Sosnick, T. R., Fang, X. & Shelton, V. M. (2000). Application of circular dichroism to study RNA folding transitions. *Methods Enzymol.* **317**, 393–409.
34. Lilley, D. M. (1999). Folding and catalysis by the hairpin ribozyme. *FEBS Letters*, **452**, 26–30.
35. Dinman, J. D. & Wickner, R. B. (1992). Ribosomal frameshifting efficiency and gag/gag-pol ratio are critical for yeast M1 double-stranded RNA virus propagation. *J. Virol.* **66**, 3669–3676.
36. Plant, E. P. & Dinman, J. D. (2005). Torsional restraint: a new twist on frameshifting pseudoknots. *Nucl. Acids Res.* **33**, 1825–1833.
37. Napthine, S., Liphardt, J., Bloys, A., Routledge, S. & Brierley, I. (1999). The role of RNA pseudoknot stem 1 length in the promotion of efficient −1 ribosomal frameshifting. *J. Mol. Biol.* **288**, 305–320.
38. Chen, X., Chamorro, M., Lee, S. I., Shen, L. X., Hines, J. V., Tinoco, I., Jr & Varmus, H. E. (1995). Structural and functional studies of retroviral RNA pseudoknots involved in ribosomal frameshifting: nucleotides at the junction of the two stems are important for efficient ribosomal frameshifting. *EMBO J.* **14**, 842–852.
39. Hansen, T. M., Reihani, S. N., Oddershede, L. B. & Sorensen, M. A. (2007). Correlation between mechanical strength of messenger RNA pseudoknots and ribosomal frameshifting. *Proc. Natl Acad. Sci. USA*, **104**, 5830–5835.
40. Namy, O., Moran, S. J., Stuart, D. I., Gilbert, R. J. & Brierley, I. (2006). A mechanical explanation of RNA pseudoknot function in programmed ribosomal frameshifting. *Nature*, **441**, 244–247.
41. Liphardt, J., Onoa, B., Smith, S. B., Tinoco, I. J. & Bustamante, C. (2001). Reversible unfolding of single RNA molecules by mechanical force. *Science*, **292**, 733–737.
42. Onoa, B., Dumont, S., Liphardt, J., Smith, S. B., Tinoco, I., Jr & Bustamante, C. (2003). Identifying kinetic barriers to mechanical unfolding of the T. thermophila ribozyme. *Science*, **299**, 1892–1895.
43. Tinoco, I., Jr, Collin, D. & Li, P. T. (2004). The effect of force on thermodynamics and kinetics: unfolding single RNA molecules. *Biochem. Soc. Trans.* **32**, 757–760.
44. Bustamante, C., Chemla, Y. R., Forde, N. R. & Izhaky, D. (2004). Mechanical processes in biochemistry. *Annu. Rev. Biochem.* **73**, 705–748.
45. Tinoco, I., Jr (2004). Force as a useful variable in reactions: unfolding RNA. *Annu. Rev. Biophys. Biomol. Struct.* **33**, 363–385.
46. Brierley, I., Digard, P. & Inglis, S. C. (1989). Characterization of an efficient coronavirus ribosomal frameshifting signal: requirement for an RNA pseudoknot. *Cell*, **57**, 537–547.
47. Bekaert, M., Bidou, L., Denise, A., Duchateau-Nguyen, G., Forest, J. P., Froidevaux, C. *et al.* (2003). Towards a computational model for −1 eukaryotic frameshifting sites. *Bioinformatics*, **19**, 327–335.
48. Kontos, H., Napthine, S. & Brierley (2001). Ribosomal Pausing at a Frameshifter RNA Pseudoknot Is Sensitive to Reading Phase but Shows Little Correlation with Frameshift Efficiency. *Mol. Cell. Biol.* **21**, 8657–8670.
49. Brierley, I., Meredith, M. R., Bloys, A. J. & Hagervall, T. G. (1997). Expression of a Coronavirus Ribosomal Frameshift Signal in Escherichia coli: Influence of tRNA Anticodon Modification on Frameshifting. *J. Mol. Biol.* **270**, 360–373.
50. Brierley, I., Rolley, N. J., Jenner, A. J. & Inglis, S. C. (1991). Mutational analysis of the RNA pseudoknot component of a coronavirus ribosomal frameshifting signal. *J. Mol. Biol.* **220**, 889–902.
51. Li, P. T., Collin, D., Smith, S. B., Bustamante, C. & Tinoco, I., Jr (2006). Probing the mechanical folding kinetics of TAR RNA by hopping, force-jump, and force-ramp methods. *Biophys. J.* **90**, 250–260.
52. Bustamante, C., Marko, J. F., Siggia, E. D. & Smith, S. (1994). Entropic elasticity of lambda-phage DNA. *Science*, **265**, 1599–1600.
53. Porschke, D. & Eigen, M. (1971). Co-operative non-enzymic base recognition. 3. Kinetics of the helix-coil transition of the oligoribouridylic–oligoriboadenylic acid system and of oligoriboadenylic acid alone at acidic pH. *J. Mol. Biol.* **62**, 361–381.
54. Collin, D., Ritort, F., Jarzynski, C., Smith, S. B., Tinoco, I., Jr & Bustamante, C. (2005). Verification of the Crooks fluctuation theorem and recovery of RNA folding free energies. *Nature*, **437**, 231–234.
55. Crooks, G. E. (1999). Entropy production fluctuation theorem and the nonequilibrium work relation for free energy differences. *Phys. Rev. E Stat. Phys. Plasmas Fluids Relat. Interdiscip. Topics*, **60**, 2721–2726.
56. Tinoco, I., Jr & Bustamante, C. (2002). The effect of force on thermodynamics and kinetics of single molecule reactions. *Biophys. Chem.* **101–102**, 513–533.
57. Bloomfield, V. A., Crothers, D. M., Tinoco, I., Jr, Hearst, J. E., Wemmer, D. E., Killman, P. A. & Turner, D. H. (2000). *Nucleic Acids: Structures, Properties, and Functions.* University Science Books, Sausalito.
58. Mathews, D. H., Sabina, J., Zuker, M. & Turner, D. H. (1999). Expanded sequence dependence of thermodynamic parameters improves prediction of RNA secondary structure. *J. Mol. Biol.* **288**, 911–940.
59. Shen, L. X. & Tinoco, I., Jr (1995). The structure of

an RNA pseudoknot that causes efficient frameshifting in mouse mammary tumor virus. *J. Mol. Biol.* **247**, 963–978.
60. Egli, M., Minasov, G., Su, L. & Rich, A. (2002). Metal ions and flexibility in a viral RNA pseudoknot at atomic resolution. *Proc. Natl Acad. Sci. USA*, **99**, 4302–4307.
61. Michiels, P. J., Versleijen, A. A., Verlaan, P. W., Pleij, C. W., Hilbers, C. W. & Heus, H. A. (2001). Solution structure of the pseudoknot of SRV-1 RNA, involved in ribosomal frameshifting. *J. Mol. Biol.* **310**, 1109–1123.
62. Wen, J. D., Manosas, M., Li, P. T., Smith, S. B., Bustamante, C., Ritort, F. & Tinoco, I., Jr (2007). Force unfolding kinetics of RNA using optical tweezers. I. Effects of experimental variables on measured results. *Biophys. J.* **92**, 2996–3009.
63. Woodside, M. T., Behnke-Parks, W. M., Larizadeh, K., Travers, K., Herschlag, D. & Block, S. M. (2006). Nanomechanical measurements of the sequence-dependent folding landscapes of single nucleic acid hairpins. *Proc. Natl Acad. Sci. USA*, **103**, 6190–6195.
64. Liphardt, J., Dumont, S., Smith, S. B., Tinoco, I., Jr & Bustamante, C. (2002). Equilibrium information from non-equilibrium measurements in an experimental test of Jarzynski's equality. *Science*, **296**, 1832–1835.
65. Smith, S. B., Cui, Y. & Bustamante, C. (2003). Optical-trap force transducer that operates by direct measurement of light momentum. *Methods Enzymol.* **361**, 134–162.

Edited by D. E. Draper

(Received 12 March 2007; received in revised form 9 May 2007; accepted 10 May 2007)
Available online 26 May 2007